



Uncertainty and sensitivity analysis of mechanical and thermal properties computed through Embedded Atom Method potential

Gurjot Dhaliwal^a, Prasanth B. Nair^b, Chandra Veer Singh^{a,c,*}

^a Department of Mechanical and Industrial Engineering, University of Toronto, Toronto, ON M5S 3G8, Canada

^b Institute of Aerospace Studies, University of Toronto, Toronto, ON M3H 5T6, Canada

^c Department of Materials Science and Engineering, University of Toronto, Toronto, ON M5S 3E4, Canada

ARTICLE INFO

Keywords:

Sensitivity analysis

Embedded Atom Method

Uncertainty quantification

ABSTRACT

Sensitivity analysis of Molecular Dynamics (MD) simulations has revealed that the predictions can be sensitive to the small perturbations in Interatomic Potential (IP) parameters. In order to make MD predictions for complex material systems more reliable, we performed uncertainty quantification of a high dimensional IP based on the Embedded Atom Method (EAM), a commonly utilized IP for metallic systems. The major contribution of this work is the prediction of a robust posterior probability distribution of the IP parameters by considering variations in the experimental values of various mechanical and thermal properties of FCC Al. The posterior probability distributions of the IP parameters were obtained using a Bayesian statistical framework. Reliability of potential parameters was assessed by performing MD simulations for a range of mechanical and thermal properties, using perturbed potential parameters. A comparison of the computed properties to existing experimental and first-principles data revealed that higher order properties such as grain boundary formation energy are sensitive (with variance of the order 10^5) to 1% perturbations. Using a Gaussian likelihood function, a posterior probability distribution of the IP parameters that minimizes the discrepancy between MD prediction and experimental values for various mechanical properties was obtained. Final properties of interest computed using this new distribution showed less sensitivity to changes in the IP parameters. Furthermore, the obtained posterior probability distribution reflects the uncertainty due to IP parameters and the quality of MD predictions is improved by propagating that uncertainty to the final properties. Thus, instead of obtaining point valued predictions from MD, probability distributions of the final properties are obtained using this framework.

1. Introduction

Atomistic simulation methods such as molecular dynamics (MD) and density functional theory (DFT) have been labeled as computational microscopes for their ability to predict physical phenomena and related properties at the nano-scale [1]. As with all models, MD models are built on certain assumptions and their accuracy is affected by their underlying structure and choice of key parameters. It has been shown that changing input parameters and conditions for these models can result in high variation in the final quantities of interest [2–4]. Hence, it is crucial to quantify and reduce the uncertainty related to corresponding model structure and parameters.

One of the key limitations of MD is its dependence on the accuracy of the Interatomic Potential (IP) function, that defines the interactions between atoms [4]. Normally, parameters of IP functions are fitted to DFT calculations and experimental results for a limited number of

conditions, leading to a bias towards certain properties or towards particular crystal structure or defects. As such, their transference to structures or property prediction outside the calibration data set can be questionable [4,5].

With the growing number of applications of MD, assessing the sensitivities of predictions with respect to IP parameters is increasingly important. Accounting for the uncertainties arising from the potential fitting procedures is also gaining attention [6–8]. Earlier work on the effect of potential parameters on final property prediction has been mostly done through sensitivity analysis (SA). In Wong et al.'s work [9], SA techniques were applied to identify the important parameters during the free energy prediction of amino acids using the Gromos potential. The results from this paper [9] led to experiments focused on accurately determining ionic charges; resulting in better potentials. Determination of important potential parameters through SA has also been the focus of a study involving Leonard Jones (LJ) liquid [10]. Kristof and Liszi [11]

* Corresponding author at: Department of Materials Science and Engineering, University of Toronto, Toronto, ON M5S 3E4, Canada.

E-mail addresses: gurjot.dhaliwal@mail.utoronto.ca (G. Dhaliwal), pbn@utias.utoronto.ca (P.B. Nair), chandraveer.singh@utoronto.ca (C.V. Singh).

applied the ideas of SA to the 3-centered model of liquid CS₂ and identified the most sensitive IP parameters leading to better fitting of these parameters. Other important SA studies focused on similar systems where the number of parameters were less than 3 [12–14]. As a proactive approach, Tschopp et al. [7] used SA methods for understanding the effect of IP parameter variability on formation energy values for the Fe-He system. The framework they provided can be used during the potential development stages, leading to robust IP parameter sets. In contrast, the present study observed that for FCC Al, lower order properties like formation energies do not vary much based on IP parameter changes; it is the higher order properties that are more sensitive. Another difference between the current work and the work done by Tschopp et al. [7], lies in the use of surrogate models, which considerably reduces the computation time as compared to full MD simulations. The effect of parameter variability on final quantities of interest (QOI) was done using ANOVA based methods for hydrocarbons by Tschopp et al. [8].

Frederiksen et al. [15], applied concepts from Bayesian statistics to estimate error bars on properties predicted through MD. They compared three different potentials and assigned independent normal likelihood to the model discrepancies from DFT or experiment values. Working along similar lines, Rizzi et al. [16] used Bayesian methods to understand the effects of parameters on the charge distribution of silica nanopores. Sensitivity of output quantities w.r.t IP parameters has also been analyzed for water [17] and in the field of biophysics [18]. As an application of Bayesian inverse methods, Rizzi et al. [19] extended their previous work in [16] by calibrating the input potential parameters using polynomial chaos expansions. Cailliez et al. [20] used Bayesian methods to calibrate the LJ potential parameters for argon, by maximizing the posterior probability. Similar methods for parameter calibration have also been implemented in [21,22] and a detailed review regarding parameter sensitivity and calibration can be found at [6,23,24].

In contrast to probabilistic uncertainty quantification methods, Tran et al. [25] used the interval based approach for uncertainty analysis in EAM potentials. This method was applied to aluminum and the stress–strain curves corresponding to different interval schemes were computed. Working on a similar material system, we applied a non-intrusive methodology and assessed the sensitivity of a number of mechanical and thermal properties.

In the present work, we study sensitivity in mechanical and thermal properties of FCC Al as predicted through the EAM potential by Mishin et al. [26]. Basic splines are fitted on tabulated values in [26] and uncertainty is introduced in the fitted parameters, followed by uncertainty propagation to the final quantities of interest (QOI). It was observed that QOI computed through EAM are sensitive to small changes in the IP parameters. On perturbing the IP parameters by 1%, basic properties such as the lattice constant remained within 0.5% of the original fitted values but higher order properties such as grain boundary formation energy showed variation as high as 85% of the original fitted values. The computational effort required for sensitivity and uncertainty analysis was eased by approximating MD simulations through models based on Gaussian processes. Using a Bayesian framework, a posterior probability distribution of each parameter which is consistent with experimental measurements of a range of mechanical and thermal properties was obtained.

High-dimensional posterior distributions were approximated through a Markov Chain Monte Carlo (MCMC) scheme. The likelihood function was designed to minimize the discrepancy between experimental values and MD predictions for a range of mechanical properties. Finally, the obtained posterior distribution was used to propagate uncertainty in the thermal properties that were not used during MCMC sampling. It was observed that probability distributions of both the property sets, mechanical and thermal, were almost normal with variance within experimental tolerance. Uncertainty Quantification models, as described in this study, capture the noise due to

experimental measurements as well as uncertainty due to fitting of IP parameters, which is propagated to QOI, thus making MD predictions more reliable.

2. Methodology

2.1. Molecular dynamics – Theory

In classical MD, the interactions between the atoms and molecules are described by Newton's equations of motion. The force acting on the i^{th} particle, F_i , can be approximated as, $F_i = -\nabla_{r_i} U(r_1, \dots, r_N)$, which is the gradient of the potential energy between N interacting atoms. One of the key components of a MD simulation is the function that approximates the interactions between the atoms. The potential function can have various functional forms like pair potentials, Embedded Atom Method (EAM) or Modified EAM [27]. Complex potentials like EAM are used to predict the properties of FCC metals. The present work focuses on EAM potential for aluminum developed by Mishin et al. [26] and considers the sensitivity of QOI w.r.t the parameters in this potential. A more detailed description of the EAM potential is provided in [supporting information](#).

2.2. Potential fitting

The EAM potential as formatted in LAMMPS setfl format [28], documents 10,000 points for embedding function. It will not be practically plausible to perform a meaningful uncertainty analysis on the 10,000 parameters. Instead, we fitted a number of spline functions to these 10,000 points and the parameters of the best spline (having lowest normalized root mean square error, 10^{-9}) are labelled as uncertain parameters. The optimal spline function generates the embedding function values for different values of the interatomic distance, which are input into LAMMPS to compute the different properties. On comparing the results from the fitted spline to the one published in [26], the maximum error was found to be less than 1.5%. The splines obtained in this manner has 11 parameters in total with 7 knots. These 11 parameters will be varied in the manner described below and their effects on the final properties will be analyzed. As these parameters are derived through spline fitting, they don't carry any physical meaning. Further, it has been shown that the choice of the spline interpolation can affect the values of certain properties of interest [29]. In this paper, we have fitted a basic spline of degree 3 with an error as low as 10^{-9} . The effect of parameters of the other interpolated splines can be part of another study, where the methods presented here can be readily applied.

2.3. Quantities of interest

We computed a number of QOI through MD simulations and studied the sensitivity of MD predictions as a function of uncertainties in the IP parameters. The details of the simulation methodology for each QOI is provided in the [supporting information](#). Details about simulation cells are documented in [Table 1](#) and atomic snapshots are as shown in [Fig. 1](#).

A summary of the methodology used for MD simulations is provided herein while more details are provided in the [supporting information](#). To compute the interstitial formation energy an extra atom is inserted at an octahedral site. The resulting structure is minimized and energy difference is recorded as Interstitial formation energy. Further, two surfaces are simulated in the cell along (001) and (00 $\bar{1}$) atomic planes and energy difference from the perfect crystal is recorded as Surface energy. Stacking fault is generated by shearing of the crystal along (112) direction. We simulated a $\Sigma 5$ grain boundary along (310) atomic plane with tilt axis along (001) direction. The misorientation angle is 34.5°.

Also, [Table 2](#) compares the values of the QOI computed using EAM to experimental, DFT and other MD studies in the literature. Comparison with other MD studies provides additional validation of the

Table 1

Details about simulation box and number of atoms for each MD simulation of FCC Aluminum. Lengths of simulations box is denoted by L_X , L_Y , L_Z . All simulations are performed at 0 K.

Properties	$L_X(A^\circ)$	$L_Y(A^\circ)$	$L_Z(A^\circ)$	Number of atoms
Cohesive energy (eV)	8.0	4.0	4.0	8
Lattice constant (A°)	8.0	4.0	4.0	8
C_{11} (GPa)	8.1	12.15	16.2	96
C_{12} (GPa)	8.1	12.15	16.2	96
C_{44} (GPa)	8.1	12.15	16.2	96
Vacancy (eV)	32.4	32.4	32.4	2048
Interstitial (eV)	32.4	32.4	32.4	2048
Surface energy (mJ/m ²)	40.5	24.3	40.5	2400
Stacking fault energy (mJ/m ²)	49.6	28.64	36.58	3200
Grain boundary (mJ/m ²)	51.23	128.07	4.05	1592

simulations conducted in this study.

2.4. Design of the UQ study

In the present work, we employ the Bayesian methodology presented in [50]. Following the same notation, we denote Y_{true} as true value of a QOI, which is related to the experimental or DFT observation value Y_{obs} through the following relation

$$Y_{obs} = Y_{true} + \epsilon_{MN}, \quad (1)$$

where ϵ_{MN} is the measurement error. For a particular IP parameter set θ , the true value of a QOI is related to the MD observation, $Y_{MD}(\theta)$ through the following relation

$$Y_{MD}(\theta) = Y_{true} + \epsilon_{MD}, \quad (2)$$

where ϵ_{MD} is the MD noise, arising due to different initial atomic velocities, autocorrelation lengths, temperature and system configurations. The goal is to find the posterior distribution of the IP parameter set θ given the observed quantity Y_{obs} , which is approximated through Bayes theorem using the equation below

$$p(\theta|Y_{obs}) \propto p(Y_{obs}|\theta)p(\theta). \quad (3)$$

To align $Y_{MD}(\theta)$ closer to Y_{obs} , the error terms ϵ_{MN} and ϵ_{MD} are combined into a single error term ϵ_{Noise} . Assuming ϵ_{Noise} to be gaussian distributed with zero mean and variance σ_{Noise}^2 , the likelihood takes the following form

$$p(Y_{obs}|\theta, \sigma_{Noise}^2) \propto \exp(-1/\sigma_{Noise}^2 [Y_{obs} - Y_{MD}]^2). \quad (4)$$

Note that computing the likelihood can be expensive and requires running a full-fledged MD simulation, which can increase the computation time. In order to circumvent this computational burden, $Y_{MD}(\theta)$ is approximated using an efficient surrogate modeling technique based on Gaussian Processes (GP) [51–53]. With applications ranging from image recognition to aerospace design, GP models are providing useful inferences to high-dimensional problems [51–53]. In the present study, training of GP models is done using MD simulation data (based on EAM potential [26]) and model performance is assessed through cross-validation measures such as the leave-one-out error and by standard cross validation residual.

Inference or output from a GP model is the mean posterior prediction $\mu_{GPM}(\theta)$ and corresponding posterior variance $\sigma_{GPM}^2(\theta)$. Incorporating these two quantities results in the following expression for the likelihood

$$p(Y_{obs}|\theta, \sigma_{Noise}^2, \sigma_{GPM}^2) \propto \exp(-[Y_{obs} - \mu_{GPM}(\theta)]\Sigma^{-1}[Y_{obs} - \mu_{GPM}(\theta)]^T), \quad (5)$$

where Σ is the diagonal matrix with each element as sum of the variance of the GP prediction, $\sigma_{GPM}^2(\theta)$ and overall noise, σ_{Noise}^2 . A MCMC scheme is used to compute the posterior distribution of the IP parameters, as detailed in the results section.

3. Results and discussion

3.1. Perturbation of IP parameters through Sobol sequence

Fitting parameters of the spline function are varied using the methodology as presented in [50]. A set of 500 points is generated using the Sobol sequence [54,55] and all the potential parameters are varied using the equations below and as presented in [50]. Based on the percentage variation, δ , a range for IP parameter set, θ , is defined as

$$\theta_{min} = \theta(1 - \delta); \quad \theta_{max} = \theta(1 + \delta) \quad \delta \in \{0.01\%, 0.1\%, 0.3\%, 0.5\%, 1\%\}, \quad (6)$$

Using the above range, each parameter is varied through the following relation

$$\theta_i = \theta_{min} + (\theta_{max} - \theta_{min})SP_i \quad i \in \{1, 2, \dots, N\}, \quad (7)$$

where SP_i is the i^{th} sobol point for a percentage variation of δ and N is the total number of stochastic IP parameters generated using the above relation. Based on the above relation, a set of $N = 500$ random vectors is generated. Each vector in the set is of dimension 11, same as number of parameters in the fitted spline. For each of the 500 vectors, MD simulations were performed using LAMMPS [28] and respective values for each QOI were obtained.

3.2. Sensitivity analysis results

We started the analysis by computing fundamental QOI such as cohesive energy and lattice constants for each setting of the IP parameters. Fig. 2 details the boxplots of these quantities at different levels of uncertainty. It can be seen that even high variations of 1% in the potential parameters lead to very small changes in the cohesive energies and lattice constant values. This observation confirms that even with the large changes, system remains physical and thus justifies the use of these potentials for the computation of higher order properties. For uncertainty levels of 1%, the values of C_{11} and C_{12} remain within 10% of the original values. C_{44} values are sensitive to the variation in the potential parameters but the range of output remains within 20% of the original values. Physical insights gained from the numerical studies are presented in the supporting information.

As shown in Fig. 3 and Table 3, QOIs such as the vacancy formation energy exhibit a maximum deviation of 23% from the original MD prediction (calculated using original parameters and reported in Table 1) while QOIs like interstitial formation energy are not that sensitive to changes in the potential parameters. A number of outliers have been observed for QOIs like surface energy and stacking fault energy at δ equal to 0.5%. As we increase the value of δ , the number of outliers keep increasing for both the quantities. Phonon conductivity computed using the Green–Kubo [56] method also showed variation with highest percentage change of 22% from the original MD prediction (Table 1). Grain boundary formation energy showed highest sensitivity with deviation as high as 293% from the original MD prediction (Table 1). Grain boundary energy values for certain parameter sets are negative in magnitude, which are not physically meaningful. For all the properties measured, the mean value of the quantity of interest remains close to the reference values, as shown by the red lines in the box plots, but variation increases as we increase the uncertainty range of the IP parameters. Using a kernel density estimation procedure [57], probability distribution of the QOI was obtained and plots are presented in supporting information.

The stress–strain response for three realizations of the random IP parameters are shown in Fig. 3(f). It can be easily verified that the change in potential parameters is accompanied by the variation in ultimate tensile strength (UTS) and failure strain (defined as the strain where fracture occurs or sharp drop in Stress–Strain curves). Uniaxial tests were performed using 10 random vectors from the stochastic potential set. For brevity, results for three of them are shown in Fig. 3(f)

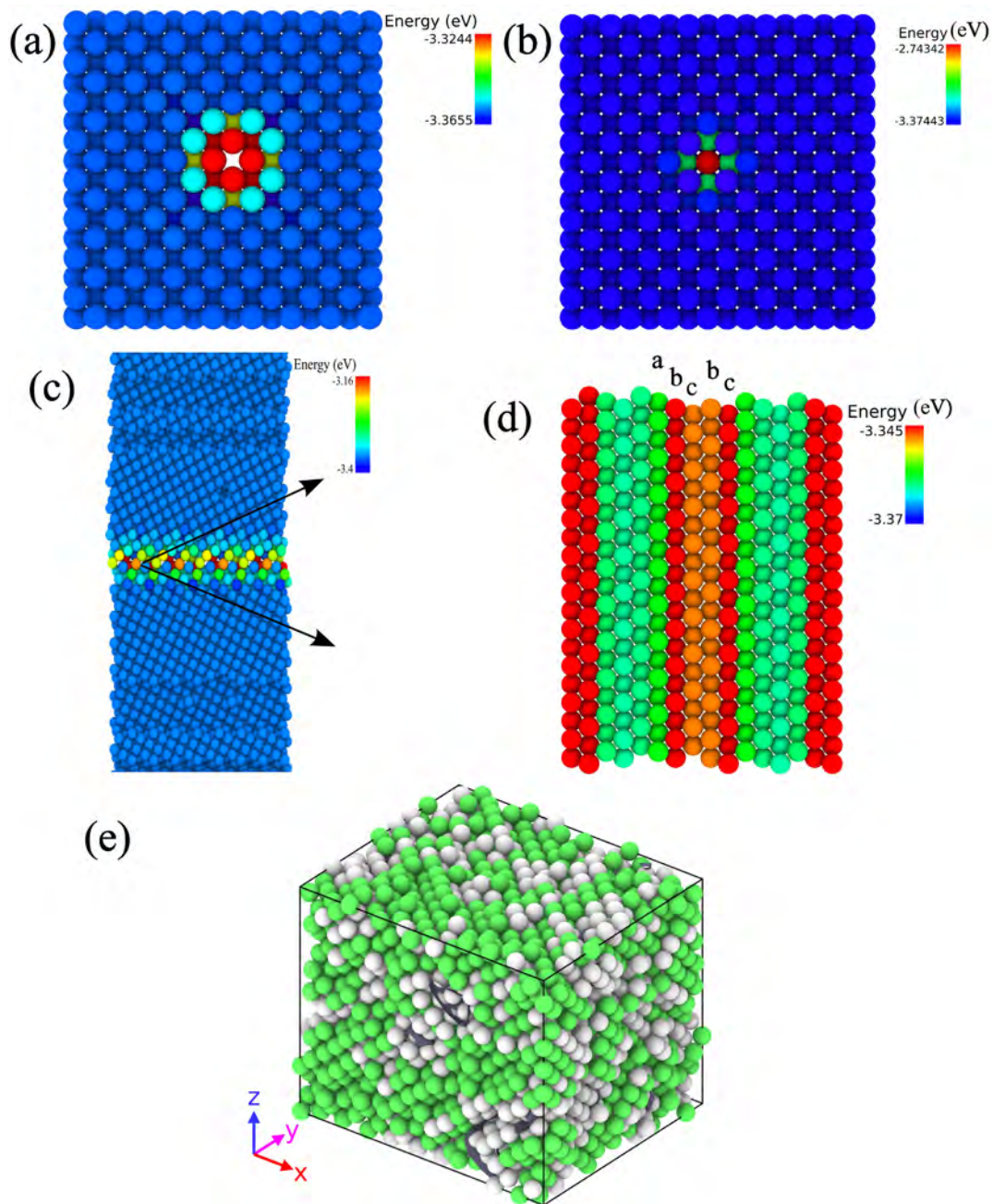


Fig. 1. Figure showing the various quantities of interest for FCC Al computed through MD simulations. Inset (a) shows the vacancy created in the simulation box. Vacancy is shown surrounded by high energy atoms (colored red). (b) Interstitial atoms (colored red) are located in one of the locations inside the lattice (c) The grain boundary is depicted by high energy atoms (colored red, green and yellow) (d) Stack fault is in the middle of simulation cell with one layer missing. (e) The simulation box under uniaxial tensile test with atoms colored according to the centro-symmetry parameter. The atoms in the grey denotes bond break with cavities nucleating around them.

and compared to the pristine curve, produced using the parameters from Mishin [26]. Although the linear region remains the same as that of the pristine curve, differences can be observed in the values of UTS and failure strain.

The focus of the present study is to analyze the sensitivity in the QOI values based on variation in the IP parameters. Apart from IP parameters, there are number of other factors, such as size of the simulation cell that may affect the QOI values and their suitable representation is necessary in every MD study. In order to evaluate the effects of these factors on the final property values, a set of MD simulations were carried out by varying size and atomic velocities. Of all the parametric studies performed on each QOI, phonon conductivity calculations

through the Green–Kubo(GK) method exhibited the highest variation. The variation is within 7% of the mean value and will be captured by σ_{Noise}^2 as described in the previous section. Considering different initial atomic velocities, system size and auto-correlation lengths, separate sensitivity analysis of phonon conductivity w.r.t variation in IP parameters was performed. It was verified that the sensitivity of phonon conductivity due to IP parameters was identical for different combinations of input factors. For brevity, sensitivity analysis is presented for a single initial atomic environment.

Table 2

A comparison of various quantities of interest computed through MD to the corresponding experimental and DFT values. The last column shows the values computed using the EAM potential [26].

Properties	Experiment	DFT	MD	MD (Mishin Potential)
Lattice constant (A°)	4.05[30,31]	4.06[32], 4.04[33]	4.05[34]	4.05
Cohesive energy (eV)	-3.36[35]	-3.42[33]	-3.36[34]	-3.36
C_{11} (GPa)	114 [36]	98 [37], 111 [38]	114.3 [39]	113.84
C_{12} (GPa)	61.9 [36]	57 [37], 56 [38]	61.9 [39]	61.59
C_{44} (GPa)	31.6 [36]	29 [37], 32 [38]	31.6 [39]	31.59
Vacancy (eV)	0.64–0.73 [34,40]	0.66 [32], 0.56 [41,42]	0.67[43], 0.68 [39]	0.676
Interstitial (eV)	3.0 [44]	2.878 [32]	2.49 [39]	2.79
Surface energy (mJ/m ²)	1,085.0 [45]		969 [43], 948 [39]	946.6
Stacking fault energy (mJ/m ²)	120 [46]	146 [47], 126 [38]	119 [34]	145.22
Grain boundary (mJ/m ²)			500 [48]	567.57
Phonon conductivity (W/mK)				11.144
UTS (GPa)				7.721
Young's modulus (GPa)	68 [49]	68 [37]	55 [37]	
Fracture strain (mm/mm)				0.1405

3.3. Correlation between inputs and outputs

To analyze the sensitivity of each QOI w.r.t each parameter, scatter plots for each combination of QOI and parameter were analyzed. Fig. 4 shows the most influential parameters and corresponding variation of the selected properties. A clear linear trend for the quantities like cohesive energy, C_{11} and C_{12} can be observed from Fig. 4. Another interesting inference can be drawn that variance is almost constant for a particular IP parameter value for these three quantities. The mean

values for cohesive energy and C_{12} are increasing as we increase θ_4 and θ_5 respectively, while value of C_{11} is decreasing as we increase θ_5 . Stack fault energy values although depicts an image of negative exponential, most of the parameter sets report values closer to 145 mJ/m².

Another method to assess the sensitivity of each parameter on the final QOI is to compute the sensitivity indices. The details to compute these indices are documented in the supporting information. Using the equations provided in supporting information, sensitivity indices were computed. It was inferred that none of the parameters were influential

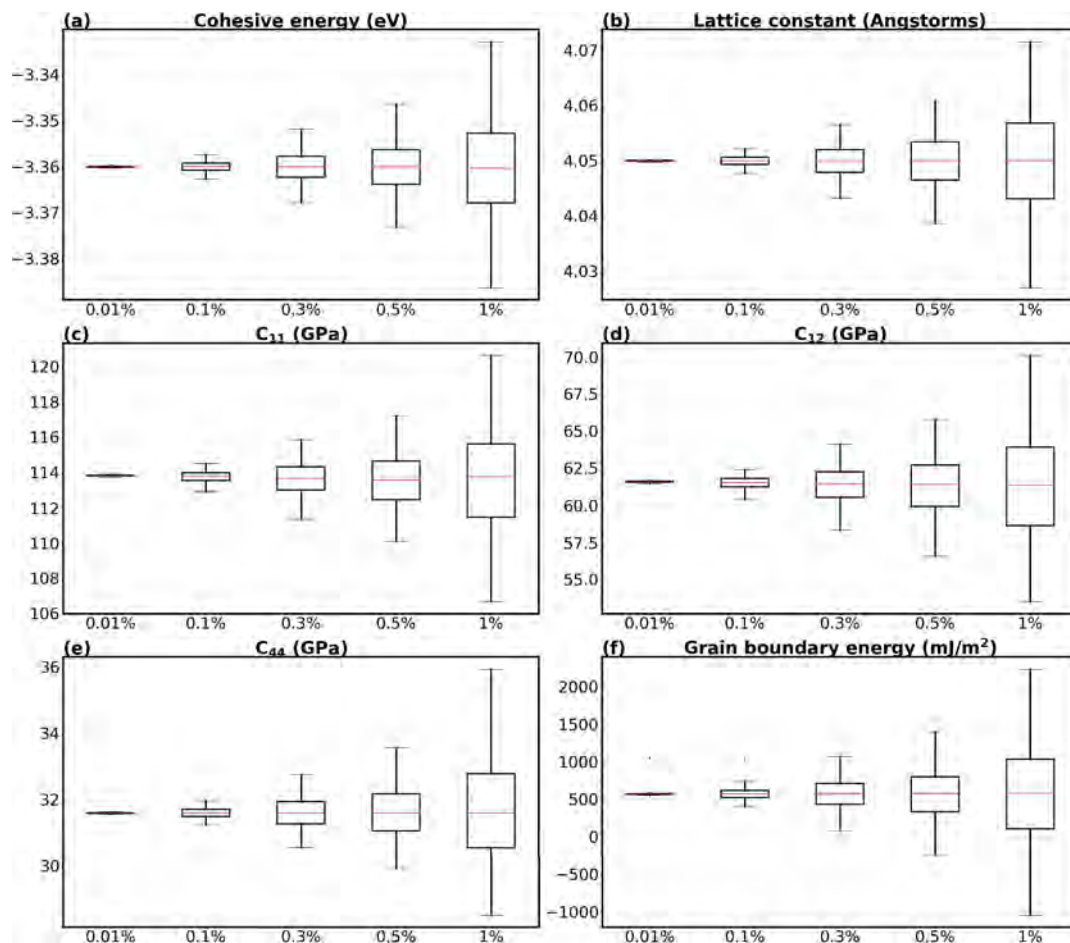


Fig. 2. Boxplots showing the results of various QOIs. Horizontal axis denotes different values of δ considered in this study. For δ equal to 1%, basic properties such as cohesive energy and lattice constant do not show high variation as compared to (e) C_{44} with 20% of variation at $\delta = 1\%$. QOI as Grain boundary formation energy exhibits a variation of the order of 10^5 at $\delta = 1\%$. The red solid line in each plot shows the mean value of each QOI obtained.

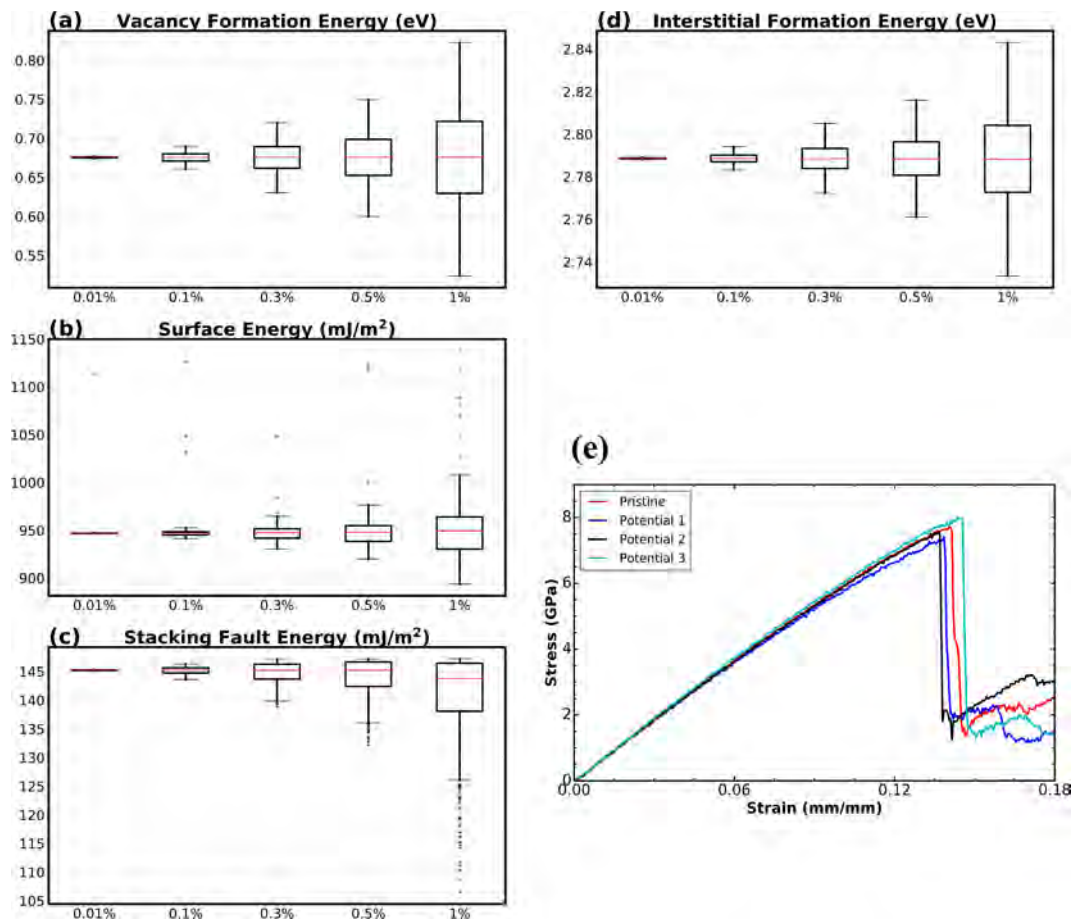


Fig. 3. Boxplots showing the variation in the various defect formation energies for Al. QOIs shown are (a) Vacancy Formation energy (b) Interstitial Formation energy (c) Surface energy (d) Stacking Fault energy (e) Stress-Strain curves for the uniaxial tensile test performed on Aluminum block. Results of three realizations are compared against the stress-strain curve obtained by using the parameters of Mishin [26] (shown in red).

for the QOI considered in the present work.

Correlation between different QOI are assessed through computation of the Pearson coefficient. Properties showed respective trends with each other that can be exploited for better IP parameters fitting. Plot of the correlations coefficients and related trends are presented in the [supporting information](#).

3.4. Gaussian process modeling

In the present work, we used GP models with zero mean prior for each QOI. Structure of the covariance function was specific to each QOI,

Table 3

Table showing the detailed results for the sensitivity analysis of various quantities of interest for 500 random potential parameters with variation(δ) of 1% from the reference values. The range column depicts the difference between minimum and maximum value of each QOI. Of all the QOI, grain boundary formation energy showed the highest variance.

Property	Mean	Minimum	Maximum	Range	Variance
Lattice constant	4.049	4.027	4.0716	0.045	10^{-5}
Cohesive energy	-3.36	-3.386	-3.333	0.054	10^{-4}
C_{11}	113.668	106.679	120.652	13.972	8.245
C_{12}	61.316	53.524	70.119	16.595	12.313
C_{44}	31.748	28.513	35.937	7.424	2.585
Phonon conductivity	11.284	9.275	13.509	4.234	0.653
Vacancy	0.675	0.524	0.823	0.299	0.004
Interstitial	2.788	2.733	2.843	0.110	0.001
Stacking fault energy	140.774	106.463	147.214	40.751	61.188
Surface energy	950.155	893.622	1137.881	244.259	818.188
Grain boundary	570.69	-1041.088	2235.16	3276.248	400612.6

as detailed in [Table 4](#). Further, performance of each GP model is assessed through cross-validation methods. In the present work, we employed Leave-one out (LOO) and standardized cross-validation residual (SCVR) methods for performance assessment.

The dataset generated using Sobol sequences has IP parameters having uniform distribution. Using a subset of the same dataset, GP models are trained for each QOI. [Fig. SI 4](#) in [supporting information](#) shows plots of GP predictions vs MD simulation result for each QOI.

[Table 4](#) shows the r-squared values of the GP predictions vs MD simulation fit for the best fitted GP model. Each QOI except surface energy shows high r-squared values depicting the linear relationship

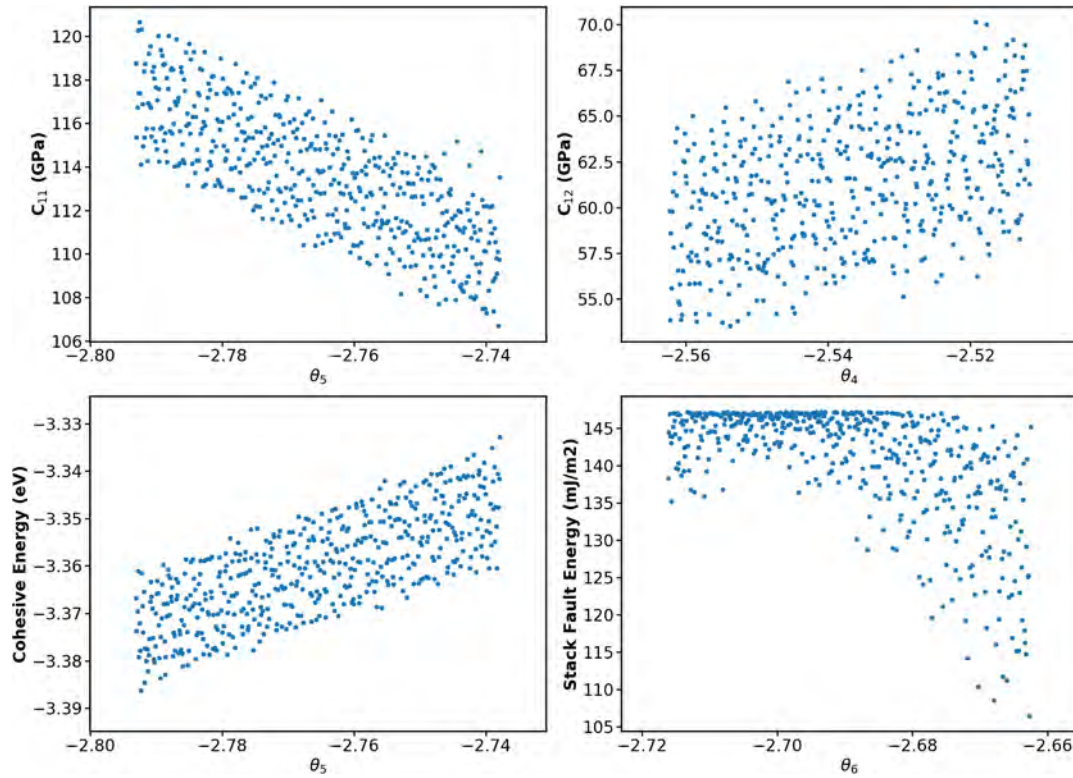


Fig. 4. Scatter plots of QOI with respect to important parameters. Not clear trends were found from the QOI vs parameter plots. IP parameter such as, θ_5 , depicts a decreasing trend for C_{11} but the same parameter shows increasing linear trend for cohesive energy.

Table 4

Root mean square error (RMSE), r-squared and normalized RMSE between GP prediction and MD prediction.

Property	Kernel	RMSE	R-Squared	Normalized RMSE
Cohesive energy	Exponential	0.011	0.982	0.196
Lattice constant	Exponential	0.0097	0.971	0.217
Vacancy	Exponential	0.061	0.841	0.202
Interstitial	Exponential	0.023	0.891	0.2066
Surface energy	Deep GP [58]	13.602	0.78	
Stacking fault energy	RBF	0.0599	0.999	0.002
C_{11}	RBF	0.454	0.975	0.033
C_{12}	Matern32	0.342	0.991	0.021
C_{44}	RBF + RBF	0.086	0.997	0.012
Grain boundary	RBF (MCMC)	26.0	0.9983	0.008

between GP predictions and corresponding MD simulations. For each property, the best surrogate model gave zero as SCVR values. Assessing the normalized root mean squared error and r-square values, it is

Table 5

Posterior distributions of the corresponding QOIs. The above QOIs are computed on the 500 points from the previous section. For notational brevity, $z(\theta)$ denotes the $\mu_{GPM}(\theta)$ in this table. The last column denotes the variance in expected value of GP prediction for a QOI.

Property	$E[z(\theta)]$	$\min(z(\theta))$	$\max(z(\theta))$	Range	$E[\sigma^2(\theta)]$	$\text{var}(z(\theta))$
Cohesive energy	-3.360	-3.385	-3.334	0.005	10^{-6}	10^{-4}
Lattice constant	4.050	4.026	4.069	0.004	10^{-7}	10^{-5}
Vacancy	0.676	0.543	0.823	0.028	10^{-5}	10^{-3}
Interstitial	2.788	2.737	2.832	0.009	10^{-6}	10^{-4}
Surface energy	948.862	901.817	1079.522	177.705	33.084	538.458
Stacking fault energy	140.795	95.982	147.252	51.27	10^{-6}	61.79
C_{11}	113.674	106.579	120.309	13.73	0.0212	7.51
C_{12}	61.323	52.058	70.479	18.42	0.014	11.67
C_{44}	31.737	28.121	36.809	8.69	10^{-5}	2.55
Grain boundary	572.761	-1036.24	2153.360	3189.6	10.476	406792.789

evident that GPs provide reliable approximation to computationally intensive MD simulations. The performance is not great for the surface energy, possibly due to the presence of large number of outliers. This issue can be dealt by considering a larger training set for this QOI. Further, the choice of covariance function also plays a significant role and the best performing covariance functions are detailed in Table 4. The last column in the table provides the normalized root mean square error of GP predictions vs. MD simulations, considering the entire set of 500 simulations. For all the properties, the error is less than 0.2.

3.4.1. Posterior predictive checks of the trained GP models

GP models developed in the last section were evaluated on the IP parameters from sensitivity analysis section. The statistics for the GP predictions of each QOI are shown in Table 5.

Comparing the GP predictions to the properties predicted through full MD simulations, we can see that $E[\mu_{GPM}(\theta)]$ differs from corresponding MD prediction by less than 0.01%, which can be easily neglected. The expected variance in the GP predictions is very low for

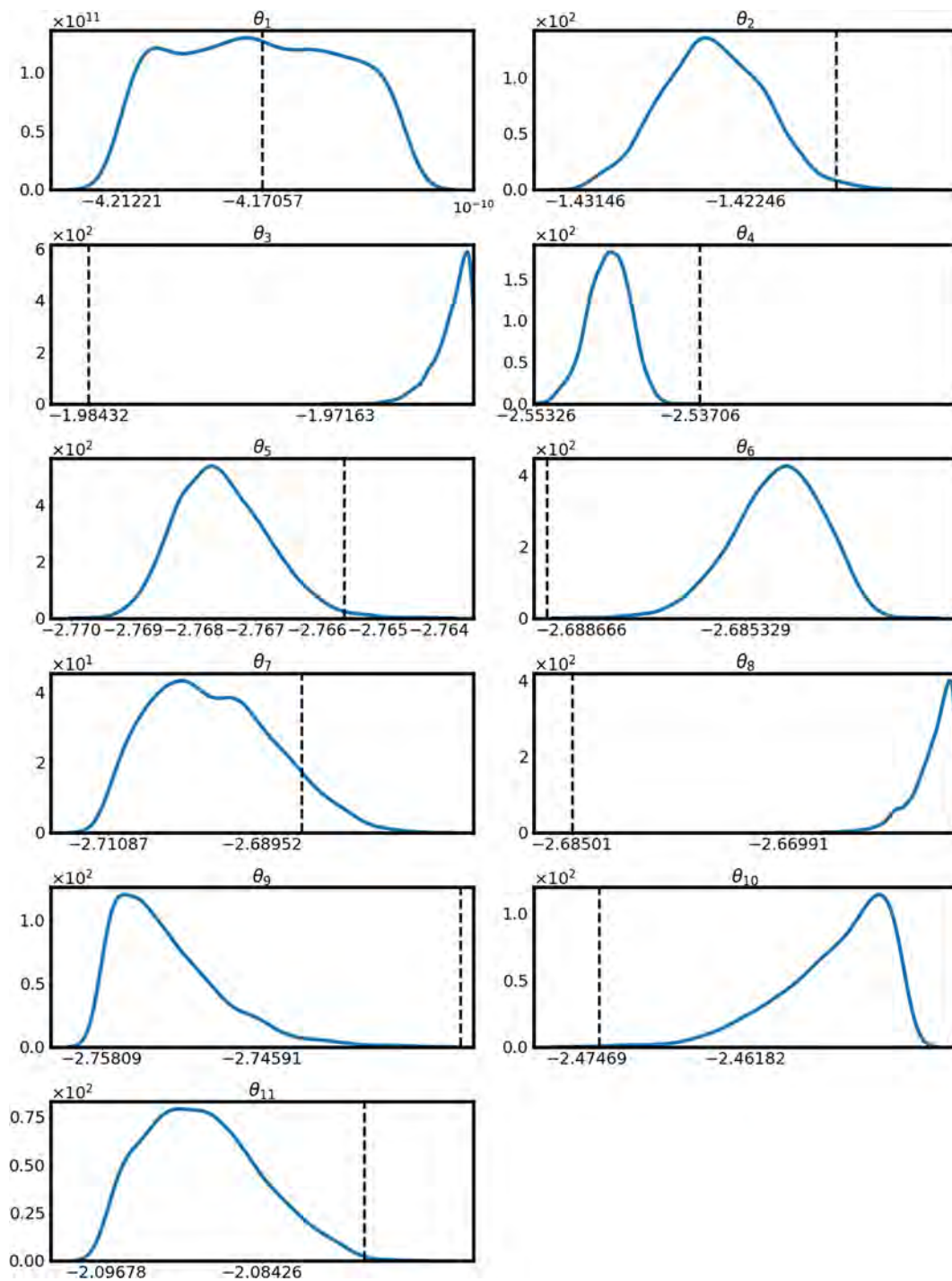


Fig. 5. Figure showing the posterior distribution of each parameter. Posterior IP parameter values are plotted along x-axis, with corresponding density distribution along y-axis. The black dashed line shows the original reference fitted value. Parameters like θ_3 , θ_4 , θ_5 , θ_6 , θ_8 had posterior probability which does not include the initial reference value. Prior used for the MCMC simulations is uniform prior with 1% variation to the initial reference values.

most of the QOI, showing that GP models are very certain about the mean values. Sensitivity in the QOI is captured through variance in the mean values, which is high for higher-order properties such as stack fault energy and grain boundary formation energy. Probability distributions for each QOI's GP prediction is obtained through kernel density estimation procedures and the plots are presented in the [supporting information](#). GP models are also used to obtain the probability of having a value of QOI within specific range. It was observed that

probabilities obtained from 10,000 GP samples were very close to the ones assessed through 500 MD simulations. Details about the probabilities are presented in [supporting information](#). Scatter plots similar to [Fig. 4](#) were obtained for GP predictions as well. GP predictions follow similar trend as observed in [Fig. 4](#), i.e. θ_5 and θ_6 contribute to highest property variation. In contrast to scatter plots, the first order sensitivity indices and total sensitivity indices do not indicate any major parameter or any significant interaction effects.

Table 6

Statistics for posterior distribution for each parameter. The first row of this table denotes the reference or the original fitted IP parameter values. Second row details the mean values of the posterior distribution of IP parameters, as obtained from MCMC scheme. The percentage change of the mean values ($\delta_{mean}\%$) from the reference values are detailed in subsequent row. Following two rows details the percentage change in minimum $\delta_{min}\%$ and maximum $\delta_{max}\%$ of the posterior distribution from the reference values.

Metric	θ_1	θ_2	θ_3	θ_4	θ_5	θ_6
Original	$-4.171e-10$	-1.417	-1.984	-2.537	-2.766	-2.689
Mean	$-4.17e-10$	-1.424	-1.956	-2.546	-2.768	-2.685
$\delta_{mean}\%$	0.02	0.49	0.95	0.36	0.07	0.18
$\delta_{min}\%$	1.0	0.99	0.64	0.64	0.15	0.027
$\delta_{max}\%$	0.99	0.27	0.99	0.065	0.05	0.28
Variance	10^{-24}	10^{-5}	10^{-7}	10^{-5}	10^{-7}	10^{-7}
Metric	θ_7	θ_8	θ_9	θ_{10}	θ_{11}	
Original	-2.684	-2.685	-2.731	-2.474	-2.076	
Mean	-2.696	-2.66	-2.753	-2.455	-2.089	
$\delta_{mean}\%$	0.46	0.94	0.82	0.78	0.62	
$\delta_{min}\%$	1.0	0.56	1.0	0.04	1.0	
$\delta_{max}\%$	0.59	1.0	0.11	0.99	0.21	
Variance	10^{-5}	10^{-7}	10^{-5}	10^{-5}	10^{-5}	

In conclusion, GPs provided a reliable and accurate approximation for the MD simulations, which can be run at a relative less computational cost. Further, a small set of MD simulations was used to train GP model, thus reducing the computational effort as required by Monte Carlo studies.

3.5. Posterior sampling through Markov Chain Monte Carlo algorithm

The posterior distribution for each parameter is approximated through a MCMC scheme using the python library PyMC3 [59]. We used a uniform distribution as prior and Gaussian likelihood as described in the previous section. Two independent MCMC chains with length 80,000, are drawn for each parameter and their convergence is assessed through various methods. From the trace plots and through computation of Geweke's indices, it was determined that chains for the parameters have converged. Additional analysis of the auto-correlation plots for different lag lengths further confirm the convergence of the MCMC chains.

Fig. 5 shows the posterior probability distribution for each parameter, with black dashed line showing the original fitted value. From the Fig. 5, it is clear that not all the parameters have the true reference value within the posterior probability distribution. High posterior density intervals for certain parameters, notably θ_5 , θ_6 do not include the original fitted parameter values. The quantitative differences between different statistics of posterior distribution with respect to the original fitted values are summarized in Table 6. Also compared are the percentage variation of the mean, minimum, maximum values of posterior from the true reference values.

Although variance of the individual posterior distribution is very low, the mean of these parameters differs as high as 0.8%. Further, the range of these parameters is as high as 1%. A possible reason for this variation is the use of experimental value of QOI. As the MCMC scheme is trying to minimize the error defined by likelihood function, only those IP parameter values are selected which can provide MD or GP model's predictions closer to the corresponding experimental values.

To perform the posterior predictive check, a sample of 1000 IP parameters are obtained from the posterior distribution and corresponding GP models are used to obtain the respective distributions of each QOI. The obtained distributions are as shown in Fig. 6. It can be observed that values for each QOI shows little scatter and percentage

change from respective mean values is less than 2%. For each QOI, Table 7 compares the mean of GP predictions, $E[\mu_{GPM}(\theta)]$, to the corresponding Y_{obs} values. It can be observed that GP predictions for most of the QOI lie closer to their respective experiment values. Variance in the GP predictions (performed for 1000 posterior IP parameters) is considerably lower than the ones presented in Table 3, thus leading to reduction in sensitivity. Further, we observed that mean of the GP predictions for stacking fault energy is different than Y_{obs} . Since GP predictions for this QOI have very low expected variance (10^{-8}), it can be concluded that this difference from Y_{obs} is either due to measurement error (captured in the expected value of measurement noise) or through the inherent uncertainty in the model structure for EAM potential.

Combining the uncertainties from GP approximation and measurement noise, QOIs like grain boundary energy, surface energy and stack fault energy were found to be highly uncertain quantities. Possible explanation for the high surface energy is that its experimental value is 1085.0 mJ/m^2 and MCMC scheme is trying to find parameters that can predict surface energy closer to corresponding experimental value. Given the functional form of the IP function, it might not be possible to reproduce experimental values of the surface energy and thus higher expected variance of GP predictions. To reduce this error, more experimental observations are needed or uncertainty due to functional form of IP functions need to be considered. Uncertainty due to functional form of IP can be reduced by using machine learning based interatomic potentials [60–62].

3.6. Posterior distribution predictions for the unknown quantity

In this section, we used the posterior distribution of the IP parameters to estimate the probability distribution of the QOI not included during MCMC sampling. Using LAMMPS, MD simulations for phonon conductivity based on Green Kubo [56] method were performed and the dataset was used to obtain a corresponding GP model. Using this GP model, probability distribution of phonon conductivity is obtained by using posterior distribution of each IP parameter. Fig. 7 details the distribution of phonon conductivity (a) for initial Sobol sample space as described in the previous sections (b) for posterior distribution as obtained through MCMC scheme.

As shown in the Fig. 7 (a), phonon conductivity values through MD showed variation of 20% from the mean values. In contrast, the probability distribution of phonon conductivity obtained by using the posterior distribution of the IP parameters depicts a maximum variation of 1.2% from the mean value.

In conclusion, the posterior distributions of the IP parameters obtained through the Bayesian framework (using MCMC) is robust towards experimental values of the QOI. Further, the new IP parameter distributions can output values of the QOI not included during MCMC sampling within measurement tolerance.

4. Conclusion

This work explored the sensitivity of output QOIs with respect to variation in interatomic potential parameters. Results from Quasi Monte Carlo schemes show that basic properties such as cohesive energy and lattice constant do not vary much with changes in the IP parameters. Conversely, defect formation energies such as grain boundary formation energy showed very high variation in their final property values. A considerable number of outliers were observed in stack fault energy and surface energy, mostly attributed to changes in atomic structure. These observations exhibit the sensitive nature of EAM potential. To identify the robust parameter sets of EAM potential, Bayesian methods were used which require large number of MD simulations. Surrogate modeling was applied to reduce the computational costs involved with MD studies. Efficient GP models reduced the

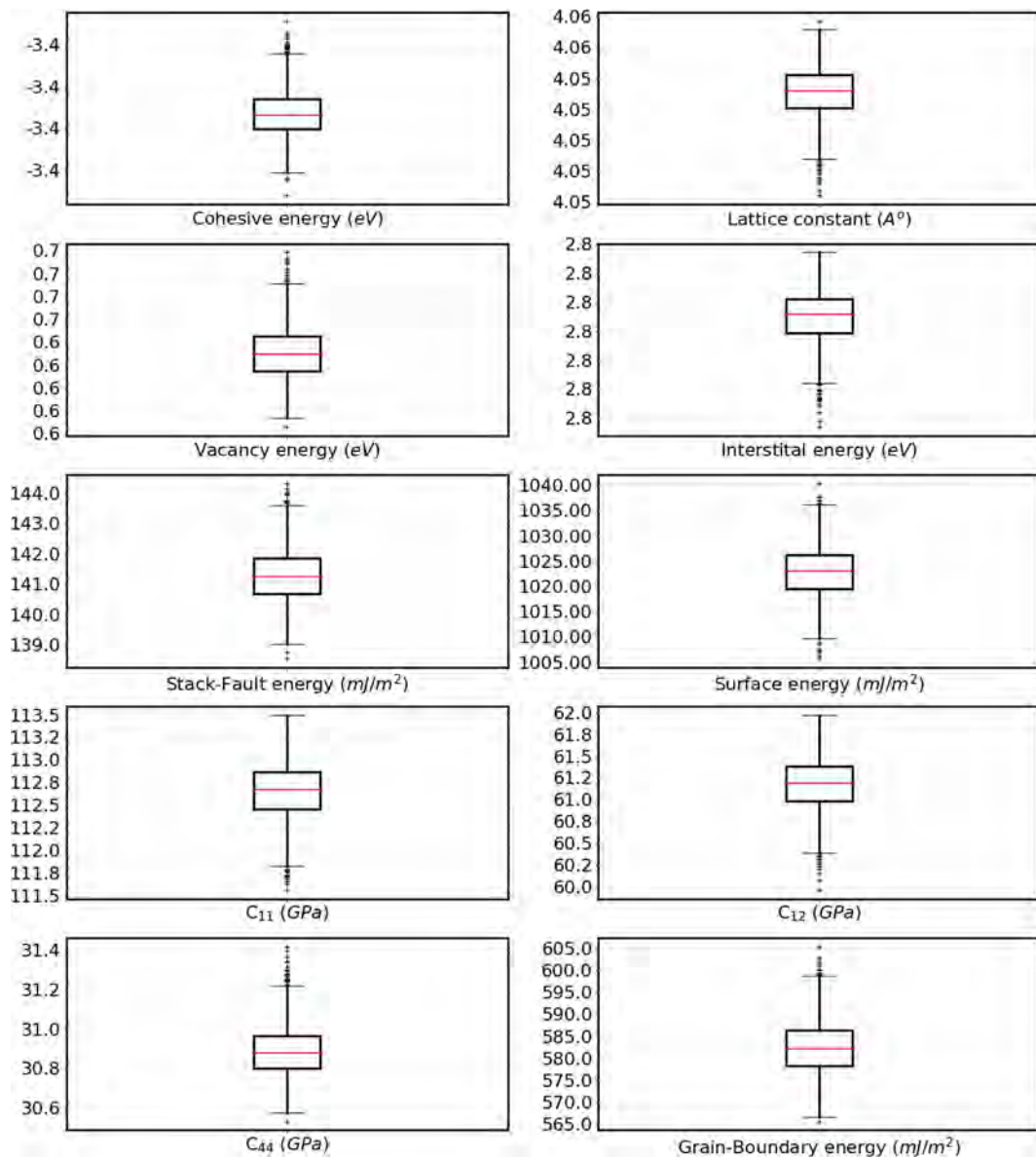


Fig. 6. Box plots of QOI w.r.t 1000 random sample points from posterior distribution of IP parameters. Values of each QOI are within experimental bounds.

Table 7

Comparison of GP predictions on a sample of size 1000 from posterior distributions of each IP parameter. First column denotes experimental values as copied from Table 2, except for grain boundary energy. For grain boundary energy, we used MD prediction by EAM potential as Y_{obs} . In comparison, $E[z(\theta)]$ values are very close to the Y_{obs} except stacking fault energy. This variance has been captured in σ_{Noise}^2 .

Property	Y_{obs}	$E[z(\theta)]$	$\text{var}(z(\theta))$	$E[\sigma_{GPM}^2(\theta)]$	$E[\sigma_{Noise}^2]$
Cohesive energy	-3.36	-3.36	10^{-8}	10^{-7}	0.092
Lattice constant	4.05	4.06	10^{-7}	10^{-7}	0.13
Vacancy	0.66	0.64	10^{-5}	10^{-5}	0.17
Interstitial	3.0	2.82	10^{-6}	10^{-6}	0.38
Stacking fault energy	120	141.29	0.74	10^{-8}	3.27
Surface energy	1085.0	1022.99	25.17	403.1	0.4
C_{11}	114	112.65	0.09	0.21	0.66
C_{12}	61.9	61.17	0.09	0.143	0.49
C_{44}	31.6	30.89	0.012	10^{-5}	0.65
Grain boundary	567.57	582.63	36.04	10.99	0.39

computational cost by requiring only one fifth of the number of simulations as required in initial sensitivity analysis. The MCMC scheme provided the posterior probability distribution of IP parameters that are robust to experimental results. Using posterior probabilities of the IP parameters, a predictive check was performed on the material property (phonon conductivity) that was not included in the training of the MCMC model. The probability distribution of phonon conductivity was within 1.2% of its mean showing less sensitivity than the analysis based on Sobol sequence. Using this framework, a reliable estimate of MD predictions can be obtained which is robust towards the variation in IP parameters.

Data availability

The raw/processed data required to reproduce these findings cannot be shared at this time as the data also forms part of an ongoing study.

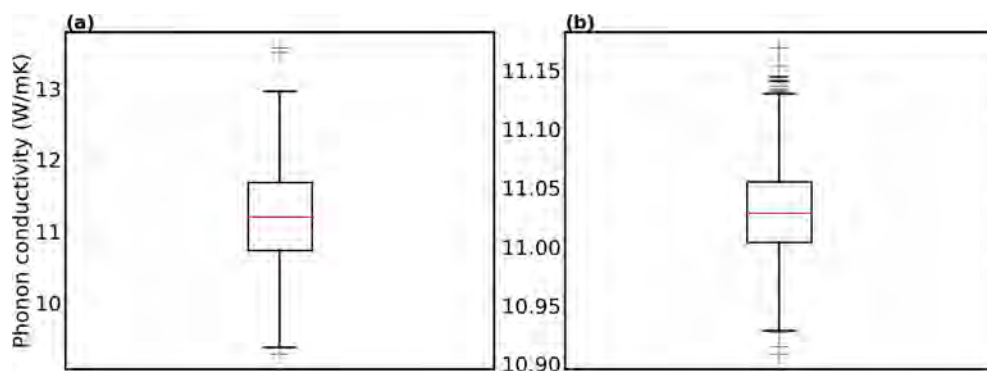


Fig. 7. Boxplot showing values of phonon conductivity at (a) Sobol sample space (b) posterior distribution of IP parameters. Phonon conductivity values were not included in initial training of MCMC scheme. Uncertainty in the IP parameters are propagated by performing MD simulations and obtaining GP predictions for phonon conductivity at 1000 IP parameters from posterior distribution.

CRedit authorship contribution statement

Gurjot Dhaliwal: Data curation, Formal analysis, Investigation, Methodology, Software, Validation, Visualization, Writing - original draft, Writing - review & editing. **Prasanth B. Nair:** Conceptualization, Investigation, Methodology, Resources, Software, Supervision, Writing - original draft, Writing - review & editing. **Chandra Veer Singh:** Conceptualization, Funding acquisition, Investigation, Methodology, Project administration, Resources, Software, Supervision, Writing - original draft, Writing - review & editing.

Acknowledgements

Support from Natural Sciences and Engineering Research Council of Canada, Hart Professorship, University of Toronto is appreciated. We are grateful to valuable resources provided by Compute Canada to perform MD simulations.

Appendix A. Supplementary data

Supplementary data associated with this article can be found, in the online version, at <https://doi.org/10.1016/j.commatsci.2019.03.060>.

References

- [1] E.H. Lee, J. Hsin, M. Sotomayor, G. Comellas, K. Schulten, Discovery through the computational microscope, *Structure* 17 (10) (2009) 1295–1306.
- [2] P.K. Schelling, S.R. Phillpot, P. Keblinski, Comparison of atomic-level simulation methods for computing thermal conductivity, *Phys. Rev. B* 65 (14) (2002) 144306.
- [3] M. Parrinello, A. Rahman, Crystal structure and pair potentials: a molecular-dynamics study, *Phys. Rev. Lett.* 45 (14) (1980) 1196.
- [4] C.A. Becker, F. Tavazza, Z.T. Trautt, R.A.B. de Macedo, Considerations for choosing and using force fields and interatomic potentials in materials science and engineering, *Curr. Opin. Solid State Mater. Sci.* 17 (6) (2013) 277–283.
- [5] C.A. Becker, F. Tavazza, L.E. Levine, Implications of the choice of interatomic potential on calculated planar faults and surface properties in nickel, *Phil. Mag.* 91 (27) (2011) 3578–3597.
- [6] Y. Wang, Uncertainty in materials modeling, simulation, and development for icme, in: *Proc. 2015 Materials Science and Technology*.
- [7] M.A. Tschopp, K. Solanki, M.I. Baskes, F. Gao, X. Sun, M. Horstemeyer, Generalized framework for interatomic potential design: application to fe–he system, *J. Nucl. Mater.* 425 (1–3) (2012) 22–32.
- [8] M.A. Tschopp, B.C. Rinderspacher, S. Nouranian, M.I. Baskes, S.R. Gwaltney, M.F. Horstemeyer, Quantifying parameter sensitivity and uncertainty for interatomic potential design: application to saturated hydrocarbons, *ASCE-ASME J. Risk Uncertainty Eng. Syst., Part B: Mech. Eng.* 4 (1) (2018) 011004.
- [9] C. Wong, H. Rabitz, Sensitivity analysis and principal component analysis in free energy calculations, *J. Phys. Chem.* 95 (24) (1991) 9628–9630.
- [10] T. Kristóf, J. Liszi, Sensitivity analysis of some thermodynamic properties of 2-centres lennard-jones liquids, *Zeitschrift für Physikalische Chemie* 190 (2) (1995) 289–297.
- [11] T. Kristóf, J. Liszi, Sensitivity analysis of the vapour-liquid phase equilibria of a model of liquid carbon disulphide, *Zeitschrift für Physikalische Chemie* 194 (2) (1996) 263–272.
- [12] S.-B. Zhu, C.F. Wong, Sensitivity analysis of water thermodynamics, *J. Chem. Phys.* 98 (11) (1993) 8892–8899.
- [13] F. Hanke, Sensitivity analysis and uncertainty calculation for dispersion corrected density functional theory, *J. Comput. Chem.* 32 (7) (2011) 1424–1430.
- [14] S.-B. Zhu, C.F. Wong, Sensitivity analysis of a polarizable water model, *The Journal*

of Physical Chemistry 98 (17) (1994) 4695–4701.

- [15] S.L. Frederiksen, K.W. Jacobsen, K.S. Brown, J.P. Sethna, Bayesian ensemble approach to error estimation of interatomic potentials, *Physical review letters* 93 (16) (2004) 165501.
- [16] F. Rizzi, R. Jones, B. Debusschere, O. Knio, Uncertainty quantification in md simulations of concentration driven ionic flow through a silica nanopore. i. sensitivity to physical parameters of the pore, *The Journal of chemical physics* 138 (19) (2013) 194104.
- [17] L.C. Jacobson, R.M. Kirby, V. Molinero, How short is too short for the interactions of a water potential? exploring the parameter space of a coarse-grained water model using uncertainty quantification, *J. Phys. Chem. B* 118 (28) (2014) 8190–8202.
- [18] B. Cooke, S.C. Schmidler, Statistical prediction and molecular dynamics simulation, *Biophysical journal* 95 (10) (2008) 4497–4511.
- [19] F. Rizzi, R. Jones, B. Debusschere, O. Knio, Uncertainty quantification in md simulations of concentration driven ionic flow through a silica nanopore. ii. uncertain potential parameters, *The Journal of chemical physics* 138 (19) (2013) 194105.
- [20] F. Cailliez, P. Pernot, Statistical approaches to forcefield calibration and prediction uncertainty in molecular simulation, *The Journal of chemical physics* 134 (5) (2011) 054124.
- [21] F. Cailliez, A. Bourasseau, P. Pernot, Calibration of forcefields for molecular simulation: Sequential design of computer experiments for building cost-efficient kriging metamodels, *Journal of computational chemistry* 35 (2) (2014) 130–149.
- [22] P. Angelikopoulos, C. Papadimitriou, P. Koumoutsakos, Data driven, predictive molecular dynamics for nanoscale flow simulations under uncertainty, *J. Phys. Chem. B* 117 (47) (2013) 14808–14816.
- [23] P. Pernot, F. Cailliez, A critical review of statistical calibration/prediction models handling data inconsistency and model inadequacy, *AIChE J.* 63 (10) (2017) 4642–4665.
- [24] A. Chernatynskiy, S.R. Phillpot, R. LeSar, Uncertainty quantification in multiscale simulation of materials: A prospective, *Annu. Rev. Mater. Res.* 43 (2013) 157–182.
- [25] A.V. Tran, Y. Wang, Reliable molecular dynamics: Uncertainty quantification using interval analysis in molecular dynamics simulation, *Comput. Mater. Sci.* 127 (2017) 141–160.
- [26] Y. Mishin, D. Farkas, M. Mehl, D. Papaconstantopoulos, Interatomic potentials for monoatomic metals from experimental data and ab initio calculations, *Phys. Rev. B* 59 (5) (1999) 3393.
- [27] M. Baskes, J. Nelson, A. Wright, Semiempirical modified embedded-atom potentials for silicon and germanium, *Phys. Rev. B* 40 (9) (1989) 6085.
- [28] S. Plimpton, Fast parallel algorithms for short-range molecular dynamics, *Journal of computational physics* 117 (1) (1995) 1–19.
- [29] M. Wen, S. Whalen, R. Elliott, E. Tadmor, Interpolation effects in tabulated interatomic potentials, *Modell. Simul. Mater. Sci. Eng.* 23 (7) (2015) 074008.
- [30] C. Kittel, P. McEuen, P. McEuen, *Introduction to solid state physics* Vol. 8 Wiley, New York, 1996.
- [31] J. Bandyopadhyay, K. Gupta, Low temperature lattice parameters of al and al-zn alloys and grüneisen parameter of al, *Cryogenics* 18 (1978) 54–55.
- [32] R. Qiu, H. Lu, B. Ao, L. Huang, T. Tang, P. Chen, Energetics of intrinsic point defects in aluminium via orbital-free density functional theory, *Phil. Mag.* 97 (25) (2017) 2164–2181.
- [33] C. Stampfl, C.G. Van de Walle, Density-functional calculations for iii–v nitrides using the local-density approximation and the generalized gradient approximation, *Phys. Rev. B* 59 (8) (1999) 5521.
- [34] K. Wang, W. Zhu, S. Xiao, J. Chen, W. Hu, A new embedded-atom method approach based on the pth moment approximation, *J. Phys.: Condens. Matter* 28 (50) (2016) 505201.
- [35] R.C. Weast, *Handbook of physics and chemistry*, CRC Press, Boca Raton, 1983–1984.
- [36] G. Simmons, Single crystal elastic constants and calculated aggregate properties, *SOUTHERN METHODIST UNIV DALLAS TEX, Tech. rep.*, 1965.
- [37] H.H. Pham, M.E. Williams, P. Mahaffey, M. Radovic, R. Arroyave, T. Cagin, Finite-temperature elasticity of fcc al: Atomistic simulations and ultrasonic measurements, *Phys. Rev. B* 84 (6) (2011) 064101.
- [38] M. Jahnátek, J. Hafner, M. Krajčí, Shear deformation, ideal strength, and stacking fault formation of fcc metals: A density-functional study of al and cu, *Phys. Rev. B* 79 (22) (2009) 224103.
- [39] B.-J. Lee, J.-H. Shim, M. Baskes, Semiempirical atomic potentials for the fcc metals cu, ag, au, ni, pd, pt, al, and pb based on first and second nearest-neighbor modified

- embedded atom method, *Phys. Rev. B* 68 (14) (2003) 144112 .
- [40] G. Hood, R. Schultz, Positron annihilation and vacancy formation in al, *J. Phys. F: Met. Phys.* 10 (4) (1980) 545.
- [41] M. Gillan, Calculation of the vacancy formation energy in aluminium, *J. Phys.: Condens. Matter* 1 (4) (1989) 689.
- [42] H. Polatoglou, M. Methfessel, M. Scheffler, Vacancy-formation energies at the (111) surface and in bulk al, cu, ag, and rh, *Phys. Rev. B* 48 (3) (1993) 1877.
- [43] M. Baskes, Modified embedded-atom potentials for cubic materials and impurities, *Phys. Rev. B* 46 (5) (1992) 2727.
- [44] P. Ehrhart, 79h2-90m Atomic Defects in Metals, Springer (1991) 372–379.
- [45] L. Mezey, J. Gibber, The surface free energies of solid chemical elements: calculation from internal free enthalpies of atomization, *Jpn. J. Appl. Phys.* 21 (11R) (1982) 1569.
- [46] R. Rautioaho, An interatomic pair potential for aluminium calculation of stacking fault energy, *physica status solidi (b)* 112 (1) (1982) 83–89.
- [47] C. Brandl, P. Derlet, H. Van Swygenhoven, General-stacking-fault energies in highly strained metallic environments: Ab initio calculations, *Phys. Rev. B* 76 (5) (2007) 054124 .
- [48] B.-J. Lee, S.-H. Choi, Computation of grain boundary energies, *Modell. Simul. Mater. Sci. Eng.* 12 (4) (2004) 621.
- [49] W.C. Oliver, G.M. Pharr, An improved technique for determining hardness and elastic modulus using load and displacement sensing indentation experiments, *Journal of materials research* 7 (6) (1992) 1564–1583.
- [50] G. Dhaliwal, P.B. Nair, C.V. Singh, Uncertainty analysis and estimation of robust airebo parameters for graphene, *Carbon* 142 (2019) 300–310.
- [51] M.C. Kennedy, A. O'Hagan, Bayesian calibration of computer models, *Journal of the Royal Statistical Society: Series B (Statistical Methodology)* 63 (3) (2001) 425–464.
- [52] A. O'Hagan, Bayesian analysis of computer code outputs: A tutorial, *Reliability Engineering & System Safety* 91 (10–11) (2006) 1290–1300.
- [53] C.E. Rasmussen, *Gaussian processes in machine learning*, in: *Advanced lectures on machine learning*, Springer, 2004, pp. 63–71.
- [54] I.M. Sobol, Uniformly distributed sequences with an additional uniform property, *USSR Computational Mathematics and Mathematical Physics* 16 (5) (1976) 236–242.
- [55] I.M. Sobol, B. Shukman, Random and quasirandom sequences: Numerical estimates of uniformity of distribution, *Mathematical and computer modelling* 18 (8) (1993) 39–45.
- [56] P.K. Schelling, S.R. Phillpot, P. Keblinski, Comparison of atomic-level simulation methods for computing thermal conductivity, *Phys. Rev. B* 65 (14) (2002) 144306 .
- [57] F. Pedregosa, G. Varoquaux, A. Gramfort, V. Michel, B. Thirion, O. Grisel, M. Blondel, P. Prettenhofer, R. Weiss, V. Dubourg, Scikit-learn: Machine learning in python, *Journal of machine learning research* 12 (2011) 2825–2830.
- [58] T. Bui, D. Hernandez-Lobato, J. Hernandez-Lobato, Y. Li, R. Turner, Deep gaussian processes for regression using approximate expectation propagation, in: *International Conference on Machine Learning*, 2016, pp. 1472–1481.
- [59] J. Salvatier, T.V. Wiecki, C. Fonnesbeck, Probabilistic programming in python using pymc3, *PeerJ Computer Science* 2 (2016) e55 .
- [60] V. Botu, R. Batra, J. Chapman, R. Ramprasad, Machine learning force fields: construction, validation, and outlook, *J. Phys. Chem. C* 121 (1) (2016) 511–522.
- [61] V. Botu, R. Ramprasad, Learning scheme to predict atomic forces and accelerate materials simulations, *Phys. Rev. B* 92 (9) (2015) 094306 .
- [62] A.P. Bartók, M.C. Payne, R. Kondor, G. Csányi, Gaussian approximation potentials: the accuracy of quantum mechanics, without the electrons, *Phys. Rev. Lett.* 104 (13) (2010) 136403 .